Rab43 regulates the sorting of a subset of membrane protein cargo through the medial Golgi

John V. Cox*, Rita Kansal, and Michael A. Whitt
Department of Microbiology, Immunology, and Biochemistry, University of Tennessee Health Science Center, Memphis, TN 38163

ABSTRACT To evaluate the role of cytoplasmic domains of membrane-spanning proteins in directing trafficking through the secretory pathway, we generated fluorescently tagged VSV G tsO45 with either the native G tail (G) or a cytoplasmic tail derived from the chicken AE1-4 anion exchanger (G^{AE}). We previously showed that these two proteins progressed through the Golgi with distinct kinetics. To investigate the basis for the differential sorting of G and G^{AE}, we analyzed the role of several Golgi-associated small GTP-binding proteins and found that Rab43 differentially regulated their transport through the Golgi. We show that the expression of GFP-Rab43 arrested the anterograde transport of G^{AE} in a Rab43-positive medial Golgi compartment. GFP-Rab43 expression also inhibited the acquisition of endoH-resistant sugars and the surface delivery of G^{AE}, as well as the surface delivery of the AE1-4 anion exchanger. In contrast, GFP-Rab43 expression did not affect the glycosylation or surface delivery of G. Unexpectedly, down-regulation of endogenous Rab43 using small interfering RNA resulted in an increase in the accumulation of G^{AE} on the cell surface while having minimal effect on the surface levels of G. Our data demonstrate that Rab43 regulates the sorting of a subset of membrane-spanning cargo as they progress through the medial Golgi.

INTRODUCTION

The trafficking of protein and lipid cargo between the compartments of the secretory pathway is dependent on their selective incorporation into newly formed transport intermediates that undergo delivery to and fusion with target membranes. These transport steps are regulated by small GTP-binding proteins of the Rab (Stenmark and Olkkonen, 2001; Zerial and McBride, 2001; Barr, 2009) and Arf/Arl (Donaldson and Honda, 2005; Kahn et al., 2006) subfamilies. These GTP-binding proteins associate with specific organelles (Pereira-Leal and Seabra, 2001; Kahn et al., 2006), where they control vesicle transport, recognition, or fusion (Chavrier et al., 1990; Zerial and McBride, 2001).

To follow the trafficking of membrane protein cargoes as they progress through the early compartments of the secretory pathway, we previously generated fluorescently tagged fusions of the tsO45 mutant of the vesicular stomatitis virus (VSV) G protein (Whitt et al., 2015). The G protein of tsO45 has a single amino acid substitution in the ectodomain that causes the protein to misfold and be retained in the endoplasmic reticulum (ER) when cells are grown at the restrictive temperature (Gallione and Rose, 1985). Fusions of tsO45 that have fluorescent protein tags (e.g., green fluorescent protein [GFP]) added to the end of the cytoplasmic tail also misfold at the restrictive temperature. However, when cells are shifted to the permissive temperature, the fusion proteins fold correctly, oligomerize, and move from the ER to the Golgi in a relatively synchronous manner (Presley et al., 1997). In experiments using fusions of VSV G tsO45 with its native cytoplasmic tail (G) or a cytoplasmic tail derived from the chicken AE1 anion exchanger (G^{AE}), we demonstrated that G and G^{AE} exhibit segregated patterns of sorting as they progress though the Golgi (Whitt et al., 2015). Furthermore, anterograde trafficking of G through early compartments of the Golgi depended on Arf1 and the COPI vesicular sorting machinery,
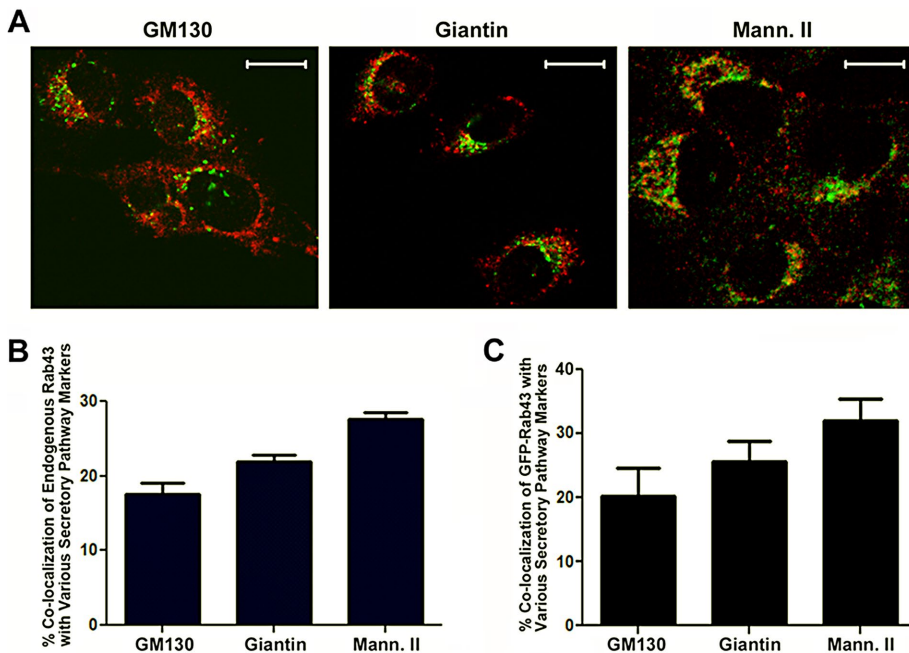
FIGURE 1: Colocalization of endogenous Rab43 with markers of the early secretory pathway. (A) PH5CH8 human hepatocytes were fixed, permeabilized, and stained with a mouse monoclonal antibody specific for Rab43 (green) and rabbit polyclonal antibodies specific for GM130, giantin, or mannosidase II (Mann. II). After incubation with the appropriate secondary antibodies, the cells were imaged by confocal microscopy. (B) Percentage colocalization of endogenous Rab43 with these various markers. (C) In similar analyses, COS7 cells were transfected with GFP-Rab43 and the percentage colocalization of this fusion with GM130, giantin, or mannosidase II (Mann. II) quantified by confocal microscopy. Average colocalization (±SD) from 25 cells from two independent experiments. Scale bars, 10 μm.

Rab43 differentially regulates the sorting of G^{AE} and G as they progress through the Golgi

Previously we showed that replacement of the cytoplasmic tail of VSV G tsO45 with a 26–amino acid sequence from the AE1-4 anion exchanger cytoplasmic domain resulted in a chimeric protein, G^{AE}, that progressed through the Golgi with kinetics distinct from that of G (Whitt et al., 2015). To determine the basis for this differential sorting, we examined whether wild-type, dominant-negative, or constitutively active, GFP-labeled, Golgi-associated small GTP-binding proteins had a differential effect on the trafficking of G or G^{AE}. The analysis included Rab1a, Rab1b, Rab2, Rab43, Arf4, and Arf5. Rab43 was the only GFP fusion assayed that had a differential effect on G and G^{AE} progression through the Golgi. Although it has been reported that a subset of GFP-Rab43 colocalizes with GM130, a cis-Golgi marker (Dejgaard et al., 2008), and TGN46 (Fuchs et al., 2007), the compartments in the early Golgi with which endogenous Rab43 associates have not been defined. Therefore we compared the localization of endogenous Rab43 to various markers of the cis- and medial Golgi in PH5CH8 human hepatocytes (Li et al., 2005), which stained best among cell lines tested with an antibody raised against human Rab43. We found that Rab43 minimally overlapped the localization profile of the cis-Golgi tether GM130 (Figure 1A). In addition, it also partially overlapped the distribution of giantin (Figure 1A), another cis-Golgi tether (Sonnichsen et al., 1998), and mannosidase II (Figure 1A), a medial Golgi marker (Velasco et al., 1993). The extent of colocalization of endogenous Rab43 with these markers can also be seen in the projections of confocal Z-stacks from single cells in Supplemental Figure S1A. Quantification of these localization studies (Figure 1B) indicated that ~15–25% of endogenous Rab43 was present in compartments containing these early Golgi markers. Similar results were obtained when we compared the localization of GFP-Rab43 to these Golgi markers in COS7 cells (Figure 1C). However, we found that a high level of expression of GFP-Rab43 resulted in a dramatic dispersal of the giantin-containing compartment and complete disruption of the mannosidase II–containing compartment (Supplemental Figure S1B). Similar fragmentation of early Golgi compartments was observed in cells overexpressing dominant-negative Rab43 (Dejgaard et al., 2008) and in cells expressing a catalytically inactive version of the GTPase-activating protein (GAP) of Rab43—RN-tre (Fuchs et al., 2007)—as well as when Rab43 is depleted in cells by siRNA (Fuchs et al., 2007). Despite these effects on Golgi organization, overexpression of wild-type GFP-Rab43 or expression of dominant-negative GFP-Rab43(T32N) in COS7 cells had no effect on the surface delivery of the VSV G tsO45 membrane glycoprotein (Dejgaard et al., 2008).

To determine the rate at which G^{AE} and G traffic through the various Golgi compartments containing endogenous Rab43, we infected PH5CH8 human hepatocytes with replication-deficient adenoviruses encoding G-DsRed or G^{AE}-DsRed and maintained the cells at the restrictive temperature of 39.8°C for 18 h. We then

as previously reported (Balch et al., 1992; Palmer et al., 1993; Hasdemir et al., 2005), whereas G^{AE} sorting through the early Golgi did not depend on Arf1 (Whitt et al., 2015).

To investigate additional possible mechanisms responsible for the distinct patterns of sorting exhibited by G and G^{AE} as they progressed through the Golgi and identify effectors that may regulate the transport of G^{AE}, we examined the effect of several small GTP-binding proteins on G^{AE} and G trafficking and found that Rab43 differentially regulated their transport. Previous studies demonstrated a role for Rab43 in the maintenance of Golgi organization (Haas et al., 2007), regulation of retrograde trafficking of cargo from the cell surface to the Golgi (Fuchs et al., 2007), and phagosome maturation in *Mycobacterium tuberculosis*–infected cells (Seto et al., 2011). Rab43 associates with multiple membrane compartments in the cell (Fuchs et al., 2007; Dejgaard et al., 2008), and our analyses revealed that expression of GFP-Rab43 arrested the anterograde transport of G^{AE} in a Rab43-containing medial Golgi compartment. In addition, GFP-Rab43 expression inhibited the acquisition of complex N-linked sugars and the surface delivery of G^{AE}, as well as the surface delivery of the AE1-4 anion exchanger, but it did not inhibit the anterograde transport of G. Down-regulation of Rab43 using small interfering RNA (siRNA) also had a selective effect on the sorting of membrane-spanning proteins, as it resulted in a significant increase in the accumulation of G^{AE} on the cell surface while having minimal effect on the surface levels of G. Collectively our results support a model in which distinct subsets of small GTP-binding proteins regulate the differential sorting of membrane-spanning proteins as they progress through the cisternae of the Golgi.
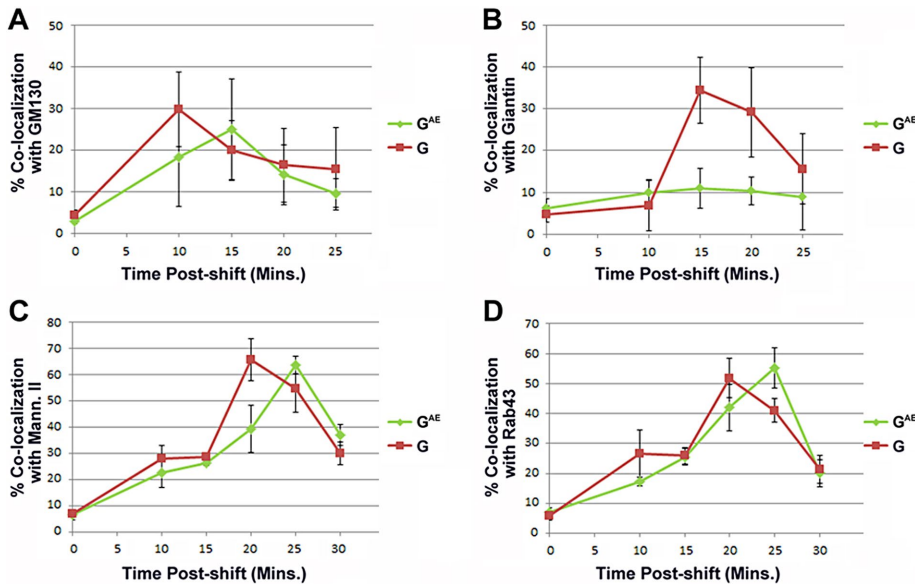
FIGURE 2: Quantification of G^{AE} and G colocalization with various markers of the early secretory pathway in PH5CH8 cells. PH5CH8 hepatocytes expressing G^{AE}-EGFP or G-EGFP were grown overnight at restrictive temperature and then shifted to permissive temperature for various times ranging from 0 to 30 min. At each time point, the cells were fixed and stained with antibodies specific for (A) GM130, (B) giantin, (C) mannosidase II, or (D) Rab43 and analyzed by confocal microscopy. The data points reflect percentage colocalization of G^{AE} or G with the various early secretory pathway markers. The colocalization values shown represent the average value obtained from Z-stacks of at least 25 different cells from two independent experiments. Additional analyses revealed that the observed differences in the colocalization of G and G^{AE} with giantin at the 15-min time point ($p < 0.0001$), with mannosidase II at the 20-min time point ($p = 0.0002$), and with endogenous Rab43 at the 25-min time point ($p = 0.0006$) were all statistically significant using the Student's two-tailed t test.

shifted the cells to the permissive temperature of 31°C for various times and compared the localization of the fusions with several markers by confocal microscopy. Similar to the results observed in COS7 and Madin–Darby canine kidney (MDCK) cells (Whitt *et al.*, 2015), G entered the GM130-containing compartment in PH5CH8 cells before G^{AE} (Figure 2A). After exiting the GM130-containing compartment, G progressed through a compartment containing giantin, whereas G^{AE} was almost entirely excluded from the giantin-containing compartment after exiting the GM130-containing compartment (Figure 2B), as previously shown in COS7 and MDCK cells (Whitt *et al.*, 2015). Although both fusions passed through the mannosidase II–containing medial Golgi, G entered and exited this compartment before G^{AE} (Figure 2C). G and G^{AE} partially overlapped the distribution of endogenous Rab43 at all of the time points examined (Figure 2D); however, the maximal colocalization of G^{AE} and G with Rab43 occurred when the fusions also maximally overlapped the localization profile of mannosidase II between 20 and 25 min after temperature shift (Figure 2, C and D).

In similar experiments, we expressed GFP-Rab43 in COS7 cells that also expressed G-DsRed or G^{AE}-DsRed. The cells were grown at restrictive temperature for 18 h, shifted to permissive temperature for 30 min, and then fixed and imaged by confocal microscopy. Although G^{AE} and G overlapped the localization of endogenous Rab43 as they traversed the Golgi in PH5CH8 cells, we found that only G^{AE} significantly colocalized with GFP-Rab43 in COS7 cells after this 30-min temperature shift (Figure 3A). Of importance, G was almost entirely excluded from GFP-Rab43–containing compartments (Figure 3B) at this time point. The differential colocalization of G^{AE} and G and with GFP-Rab43 can be more clearly seen in the

projection of confocal Z-stacks shown in Supplemental Figure S2. Quantification of G^{AE} and G colocalization with GFP-Rab43 revealed that ~70% of G^{AE} overlapped the distribution of GFP-Rab43, whereas only ~10% of G colocalized with GFP-Rab43 (Figure 3C). The lower-magnification images in Supplemental Figure S3A show this differential effect of GFP-Rab43 on G^{AE} and G in multiple COS7 cells, and similar experiments in PH5CH8 cells yielded virtually identical results (Supplemental Figure S3B).

GFP-Rab43 expression results in the accumulation of G^{AE} in the medial Golgi

We next asked whether GFP-Rab43 expression resulted in the accumulation of G^{AE} in a specific Rab43-containing subcompartment of the Golgi. Because high levels of GFP-Rab43 expression significantly altered Golgi organization (Supplemental Figure S1B), we elected to analyze the distribution of G^{AE} only in cells expressing low levels of GFP-Rab43 in order to preserve as much Golgi structure as possible. Low-level expression was defined empirically based on the relative fluorescence intensity of the GFP-Rab43 signal in transfected cells. For these studies, COS7 cells coexpressing GFP-Rab43 and G^{AE} were maintained at the restrictive temperature overnight, shifted to permissive temperature for 30 min, and then fixed and stained with antibodies directed against GM130, giantin, or mannosidase II before imaging by confocal microscopy. Analysis of these confocal slices revealed that the GFP-Rab43/G^{AE} double-positive compartment did not significantly overlap the *cis*-Golgi markers GM130 (Figure 4A) and giantin (Figures 4B and Supplemental Figure S4A), but it did overlap the localization profile of mannosidase II after a 30-min temperature shift (Figure 4C and Supplemental Figure S4A), and this pattern of localization was maintained in cells that were shifted to permissive temperature for 60 min when >80% of G^{AE} was present in a GFP-Rab43/mannosidase II double-positive compartment (Figure 3, D and E). We also found that GFP-Rab43 expression blocked the delivery of G^{AE} to the vesicle-associated membrane protein 4 (VAMP4)–positive *trans*-Golgi network (TGN) in PH5CH8 cells while having no effect on the delivery of G to this compartment (unpublished data).

In a complementary analysis, quantification of GFP-Rab43 colocalization with GM130, giantin or mannosidase II in cells coexpressing either G or G^{AE} revealed that the expression of G^{AE} induced GFP-Rab43 to accumulate in the mannosidase II–containing compartment in COS7 cells (Figure 5A). This G^{AE}-dependent redistribution of GFP-Rab43 was not observed in cells maintained at restrictive temperature (Figure 5B) and was not observed in cells expressing G at either 39.8 or 31°C (Figure 5). These results are consistent with recent studies that demonstrated a role for cargo in regulating the recruitment of sorting regulators to specific membrane compartments within cells (Caster *et al.*, 2013) and suggest that G^{AE} may interact either directly or indirectly with GFP-Rab43, resulting in the observed GFP-Rab43 redistribution.
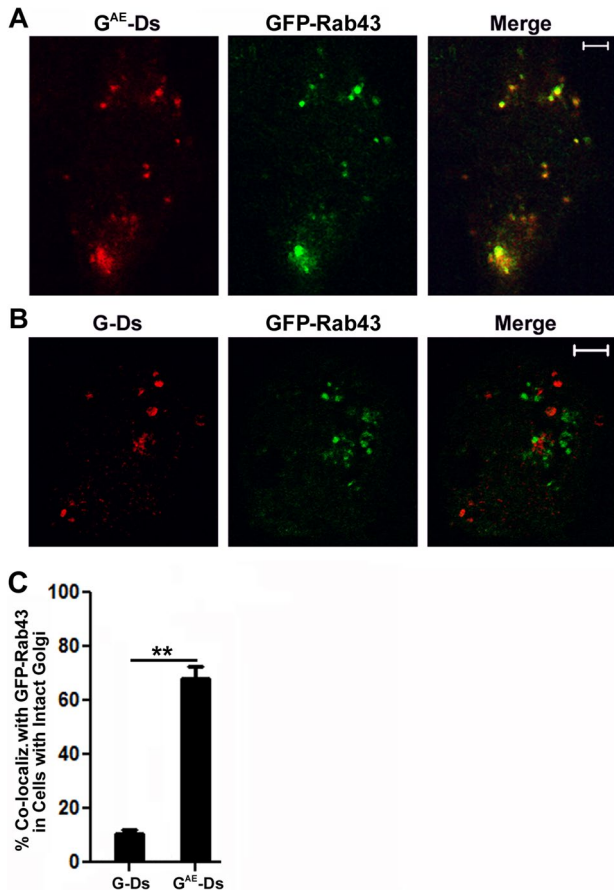
FIGURE 3: Differential effect of GFP-Rab43 on G^{AE} and G sorting. COS7 cells transfected with GFP-Rab43 were subsequently infected with replication-defective adenoviruses encoding (A) G^{AE} -Ds or (B) G-Ds and grown at the restrictive temperature for 24 h. The cells were then shifted to permissive temperature for 30 min, fixed, and imaged by confocal microscopy. The merged images show that G^{AE} accumulated in a GFP-Rab43-positive compartment, whereas G did not. (C) Percentage colocalization of G^{AE} and G with GFP-Rab43. The values represent the average (±SD) from at least 20 cells from two independent experiments. **$p < 0.0001$ (Student's two-tailed t test). Scale bars, 5 µm.

Coprecipitation of G^{AE} with GFP-Rab43

We next asked whether we could detect an interaction between G^{AE} and GFP-Rab43, which might be responsible for its accumulation in the GFP-Rab43–containing compartment. We shifted COS7 cells coexpressing GFP-Rab43 and G-DsRed or G^{AE}-DsRed to permissive temperature for 60 min and detergent lysed them in isotonic buffer containing 1% Triton X-100. Immunoblotting analysis of GFP immunoprecipitates prepared from the lysates with anti-VSV antibodies revealed that G and G^{AE} did not coprecipitate with GFP-Rab43 after detergent lysis (unpublished data), indicating the proteins did not directly interact or that the interaction was not stable in 1% Triton X-100. However, when cells were hypotonically lysed to maintain membrane integrity (Whitt *et al.*, 2015), G^{AE} coprecipitated with GFP-Rab43 (Figure 6A, lane 5), whereas G did not (Figure 6A, lane 1). The pull down of G^{AE} in this membrane precipitation assay was dependent on the expression of GFP-Rab43 (Figure 6A, lane 6) and was not observed in a precipitate prepared with control serum (Figure 6A, lane 7). It is unclear whether the ability of G^{AE} to coprecipitate with GFP-Rab43–containing membranes is due to a direct
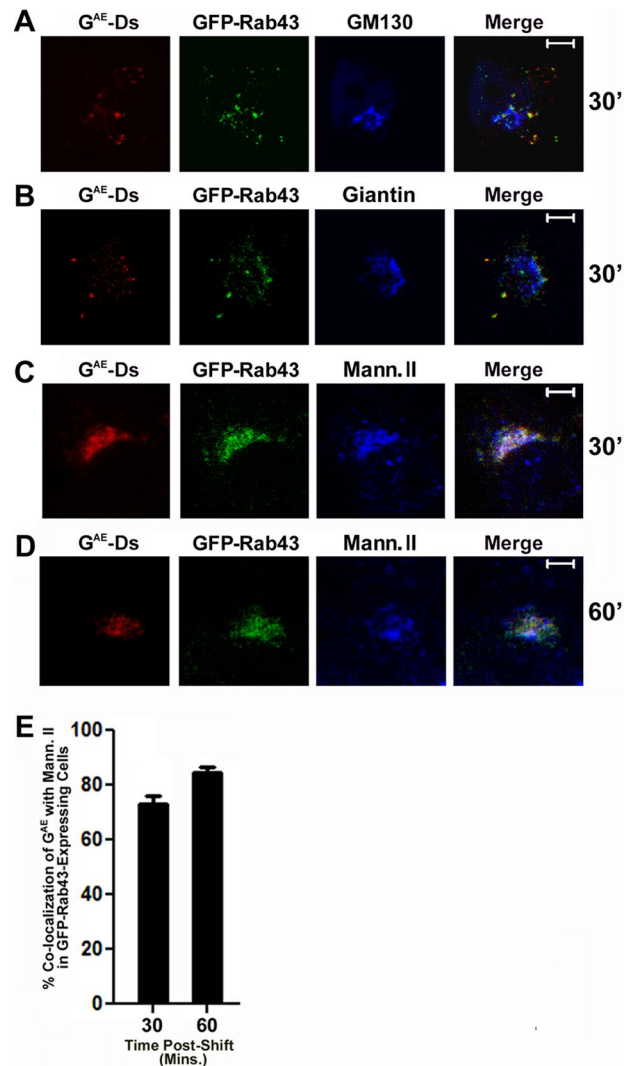

FIGURE 4: G^{AE} accumulates in a mannosidase II– and GFP-Rab43–containing compartment in GFP-Rab43–expressing cells. COS7 cells transfected with GFP-Rab43 were subsequently infected with adenovirus expressing G^{AE}-Ds and grown at the restrictive temperature for 24 h. The cells were then shifted to permissive temperature for 30 min (A–C) or 60 min (D) and fixed. The cells were then permeabilized, stained with antibodies specific for GM130 (A), giantin (B), or mannosidase II (C, D), and incubated with Alexa Fluor 647–conjugated secondary antibody. The cells were then imaged by confocal microscopy. Scale bars, 5 µm. (E) Percentage colocalization of G^{AE}-Ds with mannosidase II after a 30- or 60-min temperature shift. Average values from 20 different cells from two independent experiments.

interaction between G^{AE} and GFP-Rab43 or an interaction between G^{AE} and a GFP-Rab43–containing complex. The observed coprecipitation may also be a consequence of the two proteins residing in the same membrane microdomain.

GFP-Rab43 prevents G^{AE} complex-sugar acquisition

The observation that G^{AE} was selectively retained in the GFP-Rab43/mannosidase II–containing compartment suggested that GFP-Rab43 expression might affect the acquisition of complex N-linked sugars by G^{AE} but not by G. This possibility was tested in COS7 cells expressing GFP-Rab43. Because the expression of high levels of GFP-Rab43 disrupted Golgi organization (Supplemental Figure S1B),
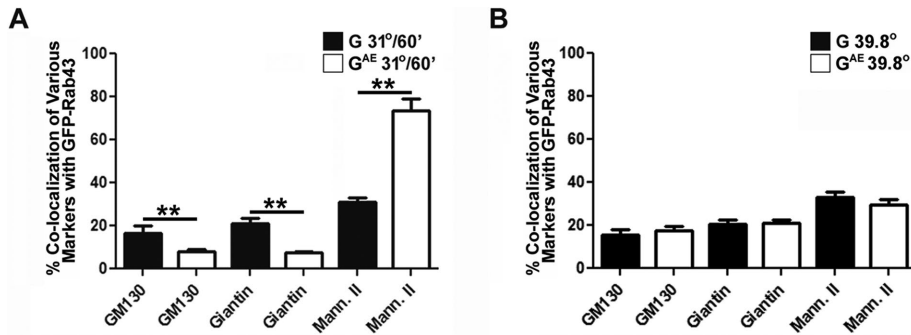
FIGURE 5: Effect of G^{AE} expression on the localization of GFP-Rab43. COS7 cells transfected with GFP-Rab43 were subsequently infected with adenoviral vectors expressing G^{AE}-Ds or G-Ds. The cells were grown at the restrictive temperature for 24 h and then shifted to permissive temperature for 60 min before fixation (A) or the cells were fixed before being shifted to permissive temperature (B). The cells were then permeabilized and stained with antibodies specific for GM130, giantin, or mannosidase II and imaged by confocal microscopy. At least 15 cells from two independent experiments were used to calculate the percentage colocalization of GFP-Rab43 with these markers of the early secretory pathway in cells expressing G^{AE}-Ds or G-Ds. **$p < 0.0001$ (Student's two-tailed t test).

we isolated COS7 cells expressing low levels of this small GTP-binding protein (Figure 6B; GFP-Rab43^{low}) by fluorescence-activated cell sorting for the analysis. The GFP-Rab43^{low} cells were infected with adenovirus encoding G^{AE} or G and grown overnight at restrictive temperature and lysed (time 0), or the cells were shifted to permissive temperature for 60 min before lysis. In each instance, the lysates were digested with endoglycosidase H and subjected to immunoblotting analysis with anti-VSV antibodies. These studies revealed that GFP-Rab43 expression almost entirely blocked the acquisition of complex N-linked sugars by G^{AE} that normally occurs when cells are shifted to permissive temperature, whereas it had minimal effect on the acquisition of complex N-linked sugars by G (Figure 6C). The conversion of N-linked sugars from simple to complex is dependent on the activity of mannosidase II in the medial Golgi (Trimble and Tarentino, 1991; Helenius and Aebi, 2001), and therefore this result was unexpected because G^{AE} appeared to accumulate in a mannosidase II–positive compartment in cells expressing GFP-Rab43 (Figure 4, C and D, and Supplemental Figure S4A). To reconcile these disparate results, we asked whether mannosidase II was present in membrane fractions containing G^{AE} and GFP-Rab43. Whereas G^{AE} coprecipitated with GFP-Rab43 (Figure 6A, lane 5), mannosidase II did not (unpublished data) indicating that despite the colocalization observed in our immunofluorescence studies, G^{AE} and GFP-Rab43 are segregated from mannosidase II in the GFP-Rab43 subcompartment of the medial Golgi, and as a consequence, the N-linked sugars on G^{AE} are not converted from simple to complex.

GFP-Rab43 prevents transport of G^{AE} and the AE1-4 anion exchanger to the cell surface

We also examined whether the retention of G^{AE} in the mannosidase II–containing compartment in GFP-Rab43–expressing cells correlated with a block in the surface delivery of this fusion in COS7 cells. For these analyses, cells expressing GFP-Rab43 and G^{AE}-Ds or G-Ds were grown at the restrictive temperature for 24 h and then shifted to permissive temperature for 60 min. The cells were then fixed, and surface G or G^{AE} was stained in nonpermeabilized cells using the I1 monoclonal antibody (Lefrancois and Lyles, 1982), which recognizes an epitope found in the G ectodomain, which is present in both of the fusions. These analyses indicated that the surface delivery of G^{AE} was inhibited in GFP-Rab43–expressing cells (Figure 7A),

but GFP-Rab43 expression had no discernible effect on the surface delivery of G (Figure 7B), an observation consistent with previous studies (Dejgaard et al., 2008). Quantification of these surface delivery assays revealed that G was transported to the cell surface with more rapid kinetics and accumulated to higher levels than surface G^{AE} (Figure 7C), as previously reported (Whitt et al., 2015). In addition, the transport of G to the plasma membrane was unaffected by GFP-Rab43 expression at any of the time points analyzed, whereas GFP-Rab43 expression significantly inhibited G^{AE} surface delivery even after a 2-h shift to permissive temperature (Figure 7C). Supplemental Figure S4B shows representative images from the 2 h-time point of this analysis.

To our knowledge, G^{AE} represents the first cargo whose anterograde transport through the secretory pathway is found to be regulated by Rab43. The cytoplasmic tail of G^{AE} was derived from the cytoplasmic domain of the chicken AE1-4 anion exchanger, and we previously showed that G^{AE} and AE1-4 have similar requirements for trafficking through the secretory pathway (Whitt et al., 2015). Therefore we next examined whether GFP-Rab43 also regulates the sorting of AE1-4. COS7 cells were cotransfected with AE1-4, which possesses an extracellular V5 epitope tag (Dorsey et al., 2007), and with GFP-Rab43, and the cells were subsequently infected with an adenoviral vector encoding G^{AE}-Ds. The cells were grown overnight at restrictive temperature, shifted to permissive temperature for 30 min, and then fixed, permeabilized, and stained with anti-V5 antibodies. In contrast to the normal cell surface pattern of localization exhibited by AE1-4 (Adair-Kirk et al., 1999; Dorsey et al., 2007), we found that the majority of AE1-4 accumulated in a compartment that was positive for both G^{AE} and GFP-Rab43 (Figure 8A), strongly suggesting that GFP-Rab43 also regulates the anterograde transport of AE1-4 through the Golgi. To investigate whether GFP-Rab43 blocked the surface delivery of AE1-4, we fixed cells transfected with V5-tagged AE1-4 and GFP-Rab43 and incubated nonpermeabilized cells with mouse anti-V5 antibodies. After washing, the cells were permeabilized and incubated with rabbit antibodies specific for the cytoplasmic domain of AE1 (Adair-Kirk et al., 1999) to detect total AE1-4. This analysis revealed that AE1-4 was retained in an intracellular GFP-Rab43–containing compartment in cells expressing the Rab43 fusion (indicated by arrows in Figure 8B), whereas it accumulated on the surface of cells that did not express GFP-Rab43 (Figure 8B). Quantification of these analyses revealed that GFP-Rab43 expression reduced surface levels of AE1-4 by ~75% (Figure 8C). The low level of surface AE1-4 detected in GFP-Rab43–expressing cells likely reflects the variable levels of GFP-Rab43 expression in cells that were analyzed. These results indicate that the pathway containing Rab43, and used by G^{AE} for progression through the Golgi, is used for the anterograde trafficking of other membrane protein cargo, including AE1-4.

Rab43 knockdown differentially affects the cell surface accumulation of G^{AE} and G

To investigate whether endogenous Rab43 differentially affects the sorting of G^{AE} and G, we down-regulated its expression in PH5CH8 cells using siRNA. Lysates prepared from cells transfected with
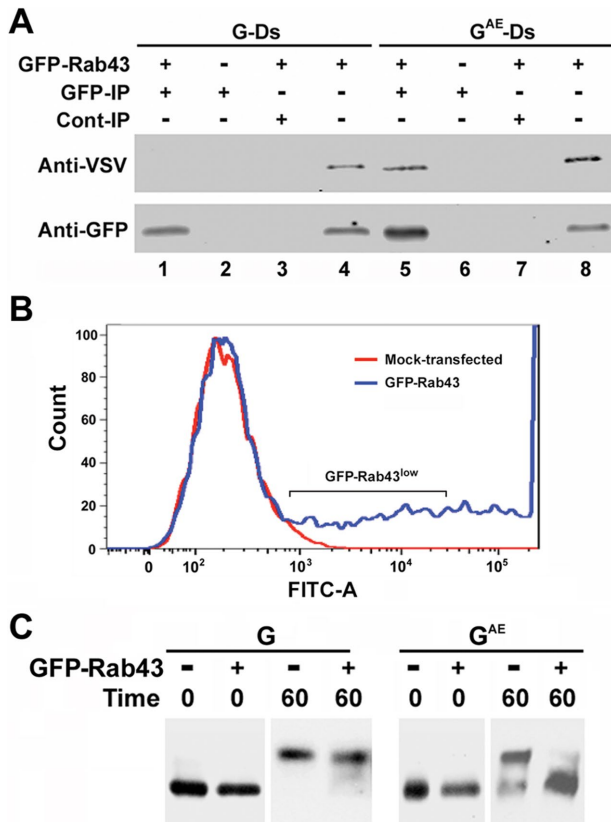
FIGURE 6: Coprecipitation of G^{AE} with GFP-Rab43. (A) COS7 cells expressing GFP-Rab43 were infected with adenovirus encoding G^{AE}-Ds or G-Ds and grown at restrictive temperature for 24 h. The cells were then shifted to permissive temperature for 60 min and harvested. After being washed in PBS, the cells were lysed by sonication and centrifuged at 5000 × g for 10 min. The supernatants were then subjected to immunoprecipitation analysis using rabbit anti-GFP (GFP) antibodies (lanes 1 and 5), and the precipitates were immunoblotted with an anti-VSV antibody that recognizes the identical ectodomains of G^{AE} and G and anti-GFP antibodies. Control GFP immunoprecipitates were prepared from cells that did not express GFP-Rab43 (lanes 2 and 6). Additional control immunoprecipitates were prepared using protein A agarose beads coated with normal rabbit serum (lanes 3 and 7). Lysates are included for comparison (lanes 4 and 8). (B) COS7 cells were transfected with GFP-Rab43, and 24 h posttransfection, cells expressing low levels of GFP-Rab43 were isolated using a fluorescence-activated cell sorter. (C) The GFP-Rab43^{low} cells or unsorted mock-transfected cells were replated and infected with adenovirus encoding G^{AE} or G. The cells were grown overnight at restrictive temperature and lysed (0 time) or shifted to permissive temperature for 60 min before lysis. In each instance, the lysates were incubated with endoglycosidase H and subjected to immunoblotting analysis with the anti-VSV antibody, which recognizes the identical ectodomains of G^{AE} and G. GFP-Rab43 expression significantly blocked the acquisition of complex N-linked sugars by G^{AE} but had minimal effect on the acquisition of complex N-linked sugars by G.

Rab43-specific siRNAs or with a scrambled control siRNA were analyzed by immunoblotting with Rab43-specific antibodies. This analysis revealed that Rab43-specific siRNAs significantly down-regulated the levels of endogenous Rab43 in PH5CH8 cells (Figure 9A). Quantification of two independent knockdowns revealed that Rab43 levels were reduced by ~90% in cells transfected with Rab43-specific siRNAs. Although previous studies indicated that Rab43 knockdown

in HeLa cells induced the dispersal of the GM130-containing cis-Golgi compartment (Fuchs et al., 2007), our localization analyses indicated that the knockdown of Rab43 in PH5CH8 cells had no obvious effect on the cellular distribution of protein disulfide isomerase, an ER marker, GM130, giantin, or VAMP4, a TGN marker (Supplemental Figure S5A). Mannosidase II, however, exhibited a more diffuse pattern of localization in approximately one-third of the cells (marked by arrows in Supplemental Figure S5A) after knockdown of Rab43 in PH5CH8 cells. Whether this diffuse staining reflects dispersal of the medial Golgi or accumulation of mannosidase II in the ER after Rab43 knockdown is unclear.

To assess the effect of Rab43 knockdown on G^{AE} and G sorting, we infected PH5CH8 cells transfected with Rab43-specific siRNAs or a control scrambled siRNA with adenovirus encoding G^{AE}–enhanced GFP (EGFP) or G-EGFP and grew them at the restrictive temperature for 24 h. The cells were then shifted to permissive temperature for 2 h, and surface G or G^{AE} was labeled by incubating intact cells at 4°C with the I1 monoclonal antibody. The resulting immune complexes were precipitated and analyzed by immunoblotting with anti-VSV antibodies. Surface G and G^{AE} were undetectable in control experiments in which the cells were maintained at the restrictive temperature of 39.8°C (Figure 9B). After the 2-h temperature shift, surface G levels were not significantly different in cells transfected with the Rab43-specific and control scrambled siRNAs. In contrast, there was a significant increase in the level of surface G^{AE} in cells transfected with the Rab43-specific siRNA compared with the control scrambled siRNA (Figure 9B). To quantify the effect of Rab43 knockdown on the surface delivery of G and G^{AE}, we carried out a fluorescence-based surface delivery assay. This analysis confirmed that the cell surface level of G after a 2-h temperature shift was minimally affected by Rab43 knockdown (Figure 9C). Furthermore, although surface G^{AE} was detectable in cells transfected with both the Rab43-specific and control scrambled siRNAs after a 2-h temperature shift (Figure 9C), the level of G^{AE} present on the cell surface at this time point was ~2.5-fold higher in Rab43-knockdown cells than in cells transfected with the control scrambled siRNA (Figure 9C), consistent with the results obtained by the surface immunoprecipitation assays (Figure 9B). Representative images from this analysis illustrate the effect of Rab43 knockdown on the surface levels of G^{AE} (Supplemental Figure S5B). The higher level of surface G^{AE} in Rab43-knockdown cells could be due to an accelerated rate of surface transport, a slower rate of internalization after surface delivery, or both. Collectively our quantitative analyses demonstrate that Rab43 regulates the trafficking of a subset of membrane-spanning proteins through the differential recognition of their cytoplasmic sequences.

DISCUSSION

Previous investigators showed that Rab43 associates with a variety of compartments within cells, including an early compartment of the Golgi, where it may be involved in regulating the association of pre-Golgi intermediates with microtubules (Dejgaard et al., 2008). It has also been shown to colocalize with GM130 (Dejgaard et al., 2008) and TGN46 (Fuchs et al., 2007) and inhibit the retrograde trafficking of Shiga-like toxins from the cell surface to the Golgi (Fuchs et al., 2007). Depletion of Rab43 by siRNA or overexpression of a catalytically inactive version of the Rab43 GAP RN-tre results in Golgi fragmentation in HeLa cells (Fuchs et al., 2007). We found that overexpression of GFP-Rab43 also resulted in dispersal of the Golgi, as visualized by immunofluorescence staining of the giantin and mannosidase-II–containing compartments (Supplemental Figure S1B), supporting the idea that Rab43 plays a critical role in the biogenesis and/or maintenance of the Golgi (Haas et al., 2007). However,
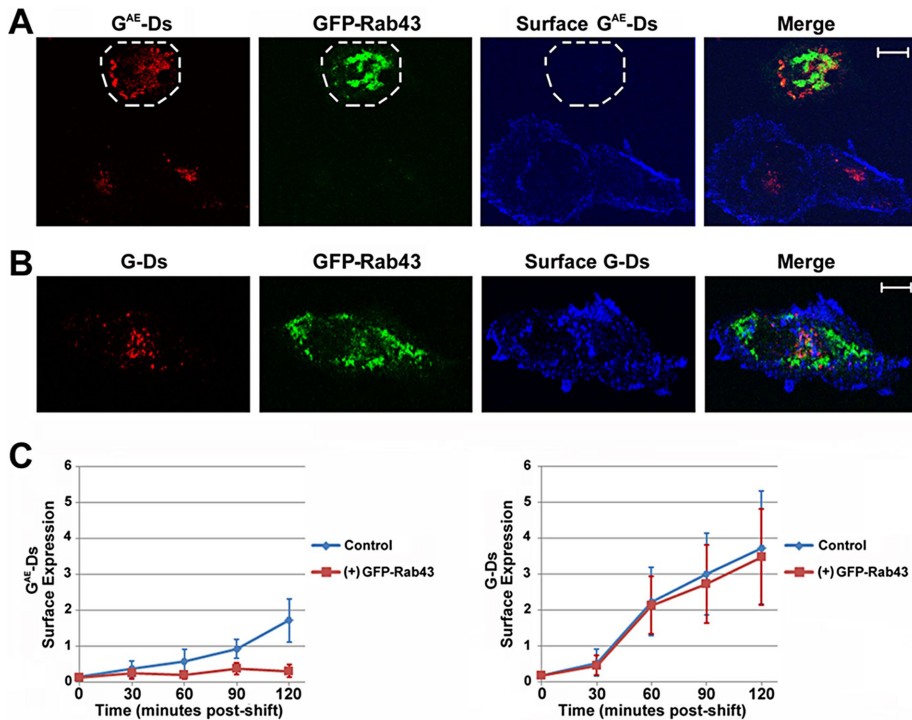
FIGURE 7: Differential effect of GFP-Rab43 on the surface accumulation of G^AE and G. COS7 cells transfected with GFP-Rab43 were subsequently infected with adenoviral vectors expressing (A) G^AE-Ds or (B) G-Ds and grown at the restrictive temperature for 24 h. The cells were then shifted to permissive temperature for 60 min and fixed. Surface G^AE or G was stained in nonpermeabilized cells using the I1 monoclonal antibody, which recognizes an epitope in the ectodomains of both G^AE and G, and an Alexa Fluor 647 secondary antibody. The cells were then imaged by confocal microscopy. The periphery of a cell coexpressing GFP-Rab43 and G^AE-Ds is outlined in A. (C) Quantification of the surface levels of G^AE-Ds and G-Ds in GFP-Rab43– expressing cells shifted to permissive temperature for times ranging from 0 to 120 min (averaged from 12–16 cells in two independent experiments). The difference in the surface delivery of G^AE-Ds at the 120-min time point in the presence and absence of GFP-Rab43 is statistically significant, with $p = 0.0003$. Scale bars, 5 μm.

whether Rab43 regulates the anterograde transport of cargo through the early secretory pathway was unknown before our studies, which analyzed sorting in the early secretory pathway using fluorescently tagged fusions of VSV G tsO45 that only differ in their cytoplasmic tails (G^AE and G). These analyses demonstrated that GFP-Rab43 expression does not affect the transit of G through the early secretory pathway or its delivery to the cell surface; however, the transport of G^AE was inhibited by GFP-Rab43 expression, which induced G^AE to accumulate in a subcompartment of the medial Golgi and prevented its surface delivery. We also found that GFP-Rab43 expression inhibited the acquisition of complex N-linked sugars by G^AE while having no effect on the glycosylation of G. The differential effect of GFP-Rab43 on G^AE and G glycosylation was somewhat puzzling because G^AE colocalized with mannosidase II in GFP-Rab43–expressing cells; however, mannosidase II was not present in membrane fractions containing GFP-Rab43 and G^AE, suggesting that the proteins are in distinct subdomains of the medial Golgi that were not resolved by our immunofluorescence studies. Although endogenous Rab43 associates with the compartment containing the cis-Golgi tether GM130 (Figure 1), G^AE progressed through this compartment in GFP-Rab43expressing cells. These results support a model of Golgi organization in which Rabs can associate with multiple cisternae but their functional activation is restricted to specific cisterna, where they can regulate the transport of defined cargo. Whereas other Rabs, including Rab33b and Rab6,

regulate Golgi organization and the retrograde trafficking of cargo from the Golgi to the ER (Darchen and Goud, 2000; Starr et al., 2010), Rab43 is the first Rab that modulates the anterograde trafficking of cargo through the medial Golgi.

The effect of GFP-Rab43 on G^AE trafficking was not unique to this membrane protein cargo, as it also affected the trafficking of the AE1-4 anion exchanger. We found that AE1-4 accumulated in the same compartment as G^AE in GFP-Rab43–expressing cells and that the surface delivery of this membrane transporter was blocked by expression of GFP-Rab43. The precise mechanism of cargo recognition by the Rab43-regulated sorting machinery remains to be defined. However, G^AE did not coprecipitate with GFP-Rab43 when cells were detergent lysed, suggesting that Rab43 may not directly interact with and regulate the transport of cargo as it progresses through the medial Golgi. In addition to the effect that GFP-Rab43 had on G^AE sorting, we also observed that the expression of G^AE influenced the distribution of GFP-Rab43 within the Golgi (Figure 5). Although others have shown that cargo can regulate the recruitment of Arf-dependent adaptor complexes to specific membrane compartments within cells (Caster et al., 2013), our data are the first to demonstrate that subclasses of cargo can specifically alter the distribution of regulatory small GTP-binding proteins within the Golgi.

The Rab43-knockdown data are consistent with activated Rab43 normally functioning to slow the rate of anterograde transport of specific cargo through the secretory pathway. This slowed rate of transport could reflect the fact that Rab43 directs a subset of cargo to subcompartments of the Golgi, where they may undergo alternative processing or maturation. Although this proposal is speculative, it could explain the fact that G^AE and G exhibit substantial differences in the way in which they acquire their complex N-linked sugar modifications as they traverse the Golgi (Whitt et al., 2015). The differential effect of Rab43 on G and G^AE sorting likely also contributes to the distinct rates of cell surface delivery exhibited by these membrane-spanning proteins (Figure 7C; Whitt et al., 2015).

Several alternative models have been proposed to account for how cargo and resident Golgi proteins are sorted through this organelle (Glick et al., 1997; Orci et al., 2000; Mironov et al., 2001; Trucco et al., 2004; Pfeffer, 2010; Lavieu et al., 2013; Rizzo et al., 2013). These models differ in whether the anterograde transport of cargo through the successive cisterna of the Golgi occurs through vesicular transport (Orci et al., 2000), cisternae-connecting tubules through which cargo could pass (Trucco et al., 2004), or cisternal maturation (Glick et al., 1997; Mironov et al., 2001). In the process of cisternal maturation, cargo and resident Golgi proteins enter the cis-most cisterna of the Golgi, and this cisterna and its proteins would progress through to the trans-face of the organelle. Resident Golgi proteins would then be retrieved from this cisterna by retrograde transport and be delivered back to specific compartments in the
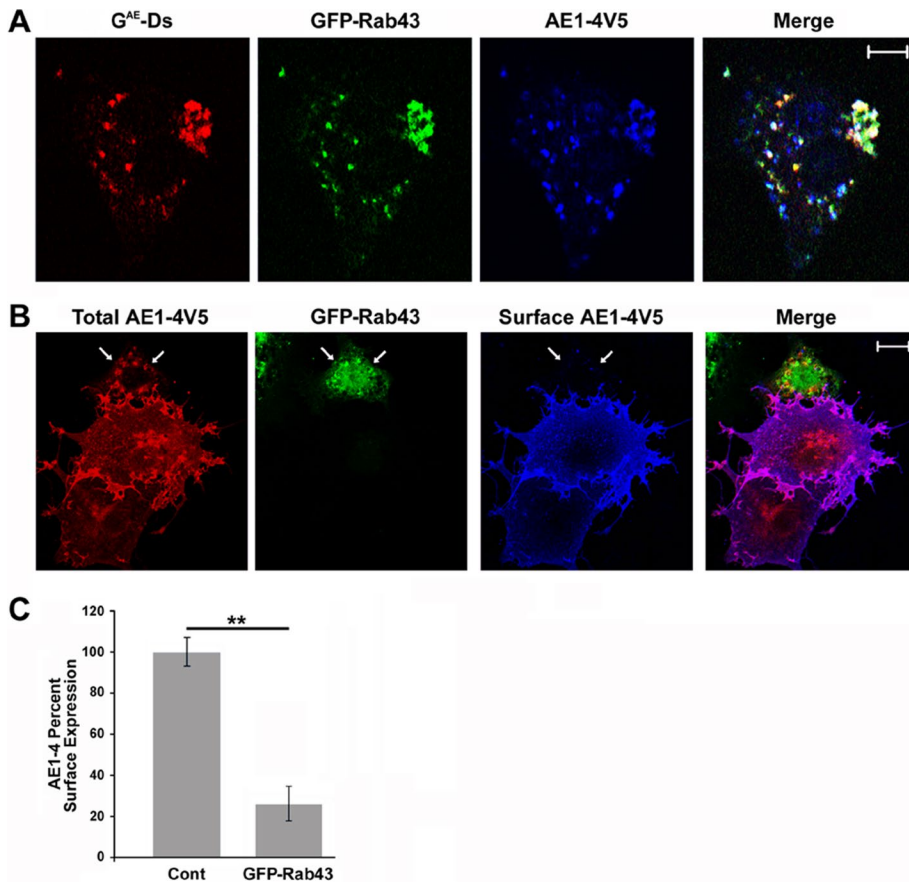
FIGURE 8: AE1-4 and G^{AE} accumulate in the same compartment in GFP-Rab43–expressing cells. (A) COS7 cells were cotransfected with AE1-4, which has an extracellular V5 epitope tag, and GFP-Rab43 and subsequently infected with an adenoviral vector encoding G^{AE}-Ds. The cells were grown overnight at restrictive temperature and then shifted to permissive temperature for 30 min, at which time the cells were fixed, permeabilized, and stained with anti-V5 antibodies. After incubation with an Alexa Fluor 647–conjugated secondary antibody, the cells were imaged by confocal microscopy. The majority of AE1-4 accumulated in a compartment that was positive for both G^{AE} and GFP-Rab43. (B) COS7 cells were cotransfected with AE1-4 containing an extracellular V5 epitope tag and GFP-Rab43. At 24 h posttransfection, the cells were fixed, and nonpermeabilized cells were incubated with mouse anti-V5 antibodies to detect AE 1-4 on the cell surface. After extensive washing, the cells were permeabilized and incubated with rabbit antibodies specific for the cytoplasmic tail of AE1 and then with goat anti-mouse secondary antibody conjugated to Alexa Fluor 647 and goat anti-rabbit secondary antibody conjugated to Alexa Fluor 594. The cells were then imaged by confocal microscopy. AE1-4 accumulated on the surface of cells that did not express GFP-Rab43. However, in cells expressing GFP-Rab43 (indicated by arrows), AE1-4 was retained in an intracellular GFP-Rab43–containing compartment. (C) Quantification of the level of surface AE1-4 in Rab43-positive and negative cells. Values reflect the average value obtained from the analysis of at least 25 cells from two independent experiments. **$p < 0.0001$ (Student's two-tailed t test). Scale bars, 5 µm.

The cisternal progenitor model for Golgi function proposes a critical role for Rabs in regulating the anterograde transport of cargo through the Golgi (Pfeffer, 2010). In this model, the successive activation and inactivation of Rabs allows for the progression of cargo through the Golgi cisternae. Inhibiting these cycles of Rab activation and inactivation is predicted to block the anterograde transport of cargo in a specific cisterna. Another feature of this model is that the activation of a Rab in one cisterna of the Golgi would allow this Rab to function in fission or fusion events in the downstream cisterna. Rab43 appears to function in a manner consistent with this model, in that it associates with both the *cis*-Golgi and medial Golgi but only regulates the anterograde transport of cargo in the more distal compartment. Although the mechanism responsible for the arrested anterograde transport of G^{AE} in GFP-Rab43–expressing cells is unclear, it may result from an effect of the GFP moiety on the GDP/GTP cycle of Rab43.

We previously demonstrated that G^{AE} and G begin to segregate soon after folding in the ER and that they progress through the Golgi with distinct kinetics (Whitt *et al.*, 2015). The different rates of transport of these two proteins through the Golgi could reflect subtle differences in the folding of the fusions upon a shift of cells to the permissive temperature. However, a more likely explanation is that the alternative cytoplasmic tails of these two fusions are differentially recognized by the cellular sorting machinery at two discrete steps during their transit through the Golgi. The transport of G through the *cis*-Golgi is dependent on Arf1 and the COPI vesicular sorting machinery, whereas the transport of G^{AE} is not (Whitt *et al.*, 2015), and the transport of G^{AE} through the medial Golgi is regulated by Rab43, whereas the transport of G is not. These results suggest that the distinct kinetics with which G^{AE} and G progress through the Golgi are due to their differential regulation by subsets of small regulatory GTP-binding proteins. Although the TGN is the

Golgi (Rizzo *et al.*, 2013), thus establishing the asymmetric distribution of resident Golgi enzymes observed in this organelle. Although all of these proposed pathways might contribute to anterograde transport of cargo through the Golgi, our data are not compatible with cisternal maturation in its simplest form, in which anterograde transport of all cargo occurs by the maturation of an intact cisterna as it moves through the organelle. The demonstration that G^{AE} and AE1-4 transport through the medial Golgi is modulated by GFP-Rab43 whereas G is not indicates that the anterograde transport of all cargo is not subject to the same regulation. Whether an alternative Rab, such as Rab41, which is involved in regulating the cell surface delivery of G (Liu *et al.*, 2013), is necessary for the anterograde transport of G through the medial Golgi is not known.

primary site where cargo is segregated into transport intermediates for delivery to alternative downstream compartments in the secretory pathway (De Matteis and Luini, 2008), our data suggest that cargo can also be partitioned during its transit through the earlier compartments of the Golgi. This partitioning in the early Golgi could result in variable access to the posttranslational modification machinery of the Golgi, which may be critical for controlling protein function.
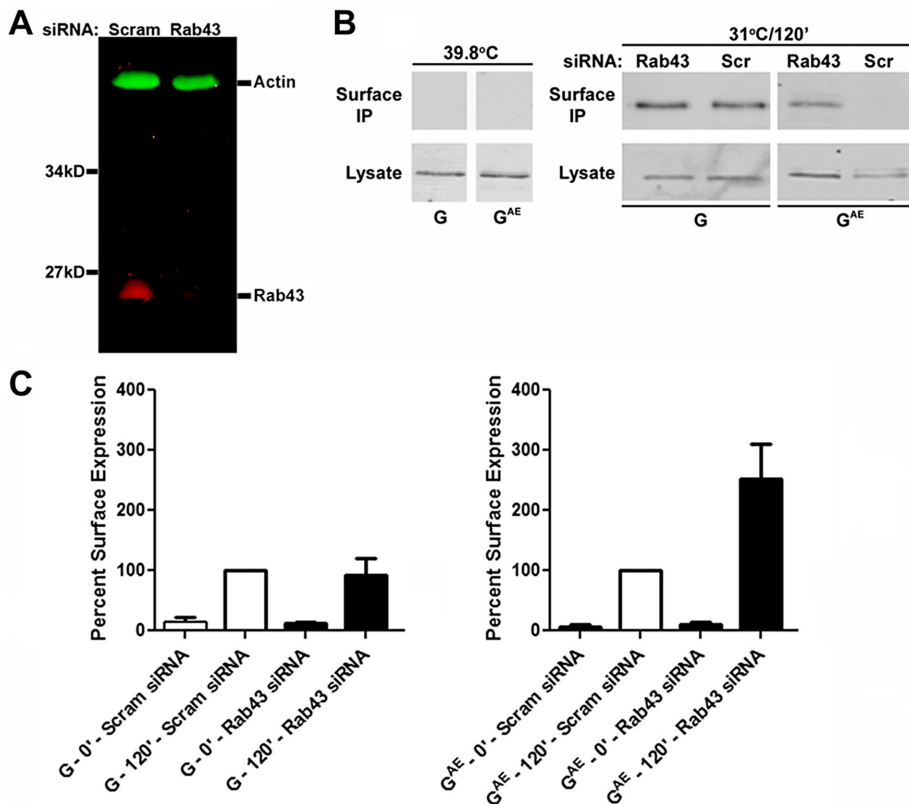
MATERIALS AND METHODS
Antibodies, reagents, and cell culture
We purchased mannosidase II rabbit polyclonal antibodies (Affinity Bioreagents, Golden, CO), Rab43 mouse monoclonal

FIGURE 9: Effect of Rab43 knockdown on G^{AE} and G trafficking. (A) PH5CH8 cells were transfected with Rab43-specific SMART pool siRNAs (12.5 nM each) or with 50 nM scrambled control siRNA, and 4 d posttransfection, the cells were harvested. Lysates were analyzed by immunoblotting analysis with Rab43-specific rabbit polyclonal antibodies and actin monoclonal antibodies. (B) PH5CH8 cells transfected with the Rab43-specific SMART pool siRNAs or with the scrambled control siRNA were infected with adenovirus encoding G^{AE}-EGFP or G-EGFP at 72 h posttransfection. After growth overnight at restrictive temperature, the cells were shifted to permissive temperature for 2 h. The cells were then shifted to 4°C and incubated with the I1 monoclonal antibody. After washing, cells were detergent lysed, and immune complexes were precipitated. The surface immunoprecipitate and lysate from each condition were analyzed by immunoblotting analysis with anti-VSV antibodies. Control experiments in which nontransfected cells were maintained at the restrictive temperature of 39.8°C are also shown. (C) PH5CH8 cells transfected with the Rab43-specific SMART pool siRNAs or with the scrambled control siRNA were infected with adenovirus encoding G^{AE}-EGFP or G-EGFP at 72 h posttransfection. After growth overnight at restrictive temperature, the cells were shifted to permissive temperature for 0 or 2 h and fixed. Surface levels of G^{AE} and G in nonpermeabilized cells were monitored by staining with the I1 monoclonal antibody, and surface-bound antibodies were detected using donkey anti-mouse immunoglobulin G conjugated to Alexa Fluor 594. The cells were imaged on a Zeiss AxioImager. M2 microscope, and the levels of surface G^{AE} and G were quantified. The values presented represent the surface fluorescence normalized to total G and G^{AE} levels at each time point.

antibodies (Abnova, Taipei City, Taiwan), Rab43 rabbit polyclonal antibodies (Atlas Antibodies, Stockholm, Sweden), VAMP4 rabbit polyclonal antibodies (Sigma-Aldrich, St. Louis, MO), and protein disulfide isomerase mouse monoclonal antibodies (ThermoFisher, Waltham, MA). V5 antibodies and the various Alexa Fluor–conjugated secondary antibodies were obtained from Invitrogen (Waltham, MA), and secondary antibodies and actin mouse monoclonal antibodies were obtained from LI-COR. Endoglycosidase H was purchased from New England Biolabs (Ipswich, MA). The polyclonal VSV (Mire *et al.*, 2010), AE1 (Adair-Kirk *et al.*, 1999), and I1 anti-G monoclonal antibodies (Lefrancois and Lyles, 1982) have been described. COS7, AD293, and PH5CH8 cells (Ikeda *et al.*, 1998) were grown in DMEM containing 10% fetal calf serum.

Plasmid and adenoviral constructs

COS7 cells or PH5CH8 cells were transfected with plasmid constructs encoding GFP-Rab43 (Dejgaard *et al.*, 2008) or V5-tagged AE1-4 (Dorsey *et al.*, 2007) using either Lipofectamine 2000 (Invitrogen) or the Effectene transfection reagent (Qiagen, Valencia, CA) according to the manufacturer's instructions. DsRed-tagged and EGFP-tagged VSV G and VSV G^{AE} constructs were cloned in the pAdEasy-1 replication-deficient adenoviral vector (Stratagene, Waltham, MA) as described (Whitt *et al.*, 2015). Viruses were grown in AD293 cells (Stratagene) and purified using the Vivapure adenoviral purification system (Sartorius, Gottingen, Germany).

Cell sorting and endoglycosidase H assays

COS7 cells were transfected with GFP-Rab43, and 24 h posttransfection, GFP-Rab43–positive cells were isolated using a FACS-Aria fluorescence-activated cell sorter. Cells expressing low levels of GFP-Rab43 or mock-transfected cells were replated and infected with adenovirus encoding G^{AE}-Ds or G-Ds. The cells were grown overnight at restrictive temperature and lysed with 1% Triton X-100 in phosphate-buffered saline (PBS) or shifted to permissive temperature for 60 min before lysis. In each instance, the lysates were incubated in the presence of endoglycosidase H according to the manufacturer's instructions, subjected to immunoblotting analysis with anti-VSV antibodies (Mire *et al.*, 2010) that recognize the identical ectodomains of G^{AE} and G, and imaged using the Supersignal West Pico Chemiluminescent reagent (Pierce, Waltham, MA).

Localization and surface delivery analyses

PH5CH8 cells were fixed with 4% paraformaldehyde in PBS. The cells were then rinsed in PBS and permeabilized with –20°C methanol before double staining with a Rab43 monoclonal antibody and rabbit polyclonal antibodies directed against GM130, giantin, or mannosidase II. After washing and incubation with the appropriate secondary antibodies, the cells were imaged using a Zeiss (Thornwood, NY) LSM510 confocal microscope. Alternatively, PH5CH8 or COS7 cells expressing GFP-Rab43 and the tagged G and G^{AE} constructs were fixed with 4% paraformaldehyde in PBS at various times after the shift to permissive temperature. The cells were then rinsed in PBS and permeabilized in PBS containing 0.1% Triton X-100 before staining with GM130, giantin, or mannosidase II antibodies. The cells were then imaged by confocal microscopy. In addition, COS7 cells expressing GFP-Rab43, V5-tagged AE1-4, and G^{AE}-Ds were grown overnight at restrictive temperature and then shifted to permissive temperature for 30 min. At this time, the cells were fixed, permeabilized, and stained with an anti-V5 antibody.

To quantify colocalization, Z-stacks were collected using a Zeiss LSM510 confocal microscope. The percentage colocalization of endogenous Rab43 or GFP-Rab43 with the various secretory pathway markers and its colocalization with G and G^{AE} were determined using the colocalization function in the Physiology package of the Zeiss LSM software from each Z-section, and total percentage colocalization for the whole cell was calculated. Similar analyses determined the percentage colocalization of G^{AE} with mannosidase II in GFP-Rab43–expressing cells. Each colocalization value is the average value obtained from Z-stacks of 15–25 different cells from two independent experiments.

For analysis of the kinetics of surface delivery of G and G^{AE} in the presence or absence of GFP-Rab43, COS7 cells were transfected with a plasmid encoding GFP-Rab43 or mock transfected with empty vector for 4 h using Lipofectamine 2000 according to the manufacturer's instruction. After removal of the transfection mix, cells were subsequently infected with adenovirus encoding G-Ds or G^{AE}-Ds and grown overnight at the restrictive temperature. The cells were then shifted to permissive temperature for various times and fixed with 4% paraformaldehyde in PBS. Nonpermeabilized cells were then incubated with the I1 monoclonal antibody, and surface bound antibodies were detected using donkey anti-mouse immunoglobulin G conjugated to Alexa 647.

To quantify G and G^{AE} surface delivery, cells expressing GFP-Rab43 and either G^{AE}-Ds or G-Ds were fixed at times ranging from 0 to 120 min after temperature shift, and nonpermeabilized cells were stained with the I1 monoclonal antibody to detect G or G^{AE} on the cell surface, followed by a secondary goat anti-mouse antibody conjugated to Alexa Fluor 647. The cells were imaged on a Zeiss LSM510 confocal microscope using the multitrack setting to individually acquire fluorescence at 488 nm (for GFP-Rab43), 543 nm (for total G-Ds or G^{AE}-Ds), and 647 nm (for I1-detected surface G or G^{AE}). Detector gain and offset values were set using the 120-min time point for G^{AE} and G separately such that no pixel saturation occurred, and all images were acquired using those settings. Images were collected at each time point using either a Plan-Neo 10×/0.3 objective with 3× digital magnification (experiment 1) or a Plan-Neo 40×/1.3 oil objective (experiment 2). Quantification was performed using the profile function to assess total (543-nm, DsRed fluorescence) and surface (647-nm fluorescence) levels of the fusions in individual cells that either did or did not express GFP-Rab43 as detected by GFP fluorescence. Relative surface expression was calculated by determining the ratio of surface (647-nm fluorescence) to total (543-nm fluorescence) G or G^{AE}. Averages and SDs were calculated from 12–16 cells/time point per experiment.

To quantify surface expression of AE 1-4, COS7 cells were cotransfected with plasmids encoding GFP-Rab43 and V5-tagged AE1-4, and at 24 h posttransfection, the cells were fixed, and nonpermeabilized cells were incubated with a mouse monoclonal anti-V5 antibody to detect the extracellular V5 epitope tag in AE1-4. The cells were then washed four times, permeabilized, and incubated with AE1-specific rabbit antibodies, which recognize an epitope on the cytoplasmic domain of AE1 (Adair-Kirk et al., 1999). Bound antibodies were detected by incubation with goat anti-mouse secondary antibody conjugated to Alexa Fluor 647 and goat anti-rabbit secondary antibody conjugated to Alexa Fluor 594, and the cells were imaged on a Zeiss LSM510 confocal microscope using the multitrack setting to collect fluorescence signals from each fluorophore separately. A strategy similar to that used to quantify surface G and G^{AE} expression was used to quantify the relative surface levels of AE1-4. A single detector and offset value was set based on the fluorescence signal from control cells that did not express GFP-

Rab43 such that no pixel saturation occurred in the brightest cells. Any cell that showed pixel saturation for either the control or the GFP-Rab43 cells was not included in the analysis. Images were collected from 25 GFP-Rab43–positive and –negative cells from two independent experiments, and the ratio of surface (647-nm fluorescence) to total (594-nm fluorescence) was used to determine surface AE1-4 levels. Percentage surface expression relative to the control (GFP-Rab43–negative) cells was calculated.

siRNA knockdowns

PH5CH8 cells were transfected with the Rab43-specific SMART pool siRNAs (12.5 nM each; Dharmacon, Lafayette, CO) or with 50 nM scrambled control siRNA using Lipofectamine RNAiMAX. Four days posttransfection, the cells were harvested, and lysates were analyzed by immunoblotting analysis with Rab43 rabbit polyclonal and actin mouse monoclonal antibodies. Immunoreactive species were detected using the LI-COR (Lincoln, NE) Odyssey imaging system. Cells were also fixed at 4 d posttransfection and stained with antibodies directed against protein disulfide isomerase, GM130, giantin, mannosidase II, or VAMP4.

For surface delivery assays, PH5CH8 cells that were transfected with the Rab43-specific SMART pool siRNAs or with the scrambled control siRNA were infected with adenovirus encoding G^{AE}-EGFP or G-EGFP at 72 h posttransfection. After growth overnight at restrictive temperature, the cells were shifted to permissive temperature for 0 or 2 h and fixed in 4% paraformaldehyde in PBS. Nonpermeabilized cells were stained with the I1 monoclonal antibody, and surface-bound antibodies were detected with goat anti-mouse secondary antibodies conjugated to Alexa Fluor 594. The fluorescence intensity resulting from this surface staining was normalized to the total amount of G^{AE}-EGFP or G-EGFP expressed in the cells as described before, except that images were captured using a Zeiss AxioCam MRm digital camera fitted on a Zeiss AxioImager.M2 epifluorescence microscope. Image acquisition was performed using the multidimensional function of the AxioVision 4.0 software for separate fluorescence channel acquisition. A single acquisition time was set using the 120-min time in the control (scrambled siRNA) sample for G and in the Rab43 siRNA transfected sample for G^{AE}, since the latter showed brighter fluorescence than the control (scrambled siRNA) sample. Percentage surface expression was then calculated using the 120-min time point of the control (scrambled siRNA) samples for both G and G^{AE}, and the values presented represent the normalized fluorescence from 8 (for G) to 20 (for G^{AE}) fields acquired with an AchroPlan immersible 40× objective for each time point. Essentially identical results were obtained in two independent experiments. Alternatively, surface delivery was assessed by an immunoblotting assay. PH5CH8 cells transfected with the Rab43-specific or control scrambled siRNAs were shifted to permissive temperature for 2 h. At this time, the cells were incubated with the I1 monoclonal antibody at 4°C for 30 min. After four washes in 4-(2-hydroxyethyl)-1-piperazineethanesulfonic acid–buffered medium (Opti-MEM), the cells were lysed in PBS containing 1% Triton X-100. Immune complexes were captured by incubating the lysates with protein A agarose beads (Repligen) and analyzed by immunoblotting analysis with the anti-VSV antibody.

Coprecipitation assays

COS7 cells expressing G-DsRed or G^{AE}-DsRed alone or coexpressing GFP-Rab43 and G-DsRed or G^{AE}-DsRed were shifted to permissive temperature for 60 min and detergent lysed in isotonic buffer containing 1% Triton X-100. Immunoprecipitates were prepared from the lysates using protein A agarose beads preloaded with

rabbit anti-GFP antibodies. Control immunoprecipitates were prepared using protein A agarose beads coated with normal rabbit serum. In each instance, precipitates were analyzed by immunoblotting analysis with VSV, GFP, and mannosidase II antibodies.

COS7 cells expressing G-DsRed or G^{AE}-DsRed alone or coexpressing GFP-Rab43 and G-DsRed or G^{AE}-DsRed were shifted to permissive temperature for 60 min, harvested by scraping, and hypotonically lysed as described previously (Whitt *et al.*, 2015). Immunoprecipitates were prepared from the hypotonic lysates using anti-GFP protein A agarose beads or beads coated with normal rabbit serum. Precipitates were then subjected to immunoblotting analysis using VSV, GFP, and mannosidase II antibodies.

REFERENCES
Adair-Kirk TL, Cox KH, Cox JV (1999). Intracellular trafficking of variant chicken kidney AE1 anion exchangers: role of alternative NH(2) termini in polarized sorting and Golgi recycling. J Cell Biol 147, 1237–1248.

Balch WE, Kahn RA, Schwaninger R (1992). ADP-ribosylation factor is required for vesicular trafficking between the endoplasmic reticulum and the cis-Golgi compartment. J Biol Chem 267, 13053–13061.

Barr FA (2009). Rab GTPase function in Golgi trafficking. Semin Cell Dev Biol 20, 780–783.

Caster AH, Sztul E, Kahn RA (2013). A role for cargo in Arf-dependent adaptor recruitment. J Biol Chem 288, 14788–14804.

Chavrier P, Vingron M, Sander C, Simons K, Zerial M (1990). Molecular cloning of YPT1/SEC4-related cDNAs from an epithelial cell line. Mol Cell Biol 10, 6578–6585.

Darchen F, Goud B (2000). Multiple aspects of Rab protein action in the secretory pathway: focus on Rab3 and Rab6. Biochimie 82, 375–384.

De Matteis MA, Luini A (2008). Exiting the Golgi complex. Nat Rev Mol Cell Biol 9, 273–284.

Dejgaard SY, Murshid A, Erman A, Kizilay O, Verbich D, Lodge R, Dejgaard K, Ly-Hartig TB, Pepperkok R, Simpson JC, et al. (2008). Rab18 and Rab43 have key roles in ER-Golgi trafficking. J Cell Sci 121, 2768–2781.

Donaldson JG, Honda A (2005). Localization and function of Arf family GTPases. Biochem Soc Trans 33, 639–642.

Dorsey FC, Muthusamy T, Whitt MA, Cox JV (2007). A novel role for a YXXPhi motif in directing the caveolin-dependent sorting of membrane-spanning proteins. J Cell Sci 120, 2544–2554.

Fuchs E, Haas AK, Spooner RA, Yoshimura S, Lord JM, Barr FA (2007). Specific Rab GTPase-activating proteins define the Shiga toxin and epidermal growth factor uptake pathways. J Cell Biol 177, 1133–1143.

Gallione CJ, Rose JK (1985). A single amino acid substitution in a hydrophobic domain causes temperature-sensitive cell-surface transport of a mutant viral glycoprotein. J Virol 54, 374–382.

Glick BS, Elston T, Oster G (1997). A cisternal maturation mechanism can explain the asymmetry of the Golgi stack. FEBS Lett 414, 177–181.

Haas AK, Yoshimura S, Stephens DJ, Preisinger C, Fuchs E, Barr FA (2007). Analysis of GTPase-activating proteins: Rab1 and Rab43 are key Rabs required to maintain a functional Golgi complex in human cells. J Cell Sci 120, 2997–3010.

Hasdemir B, Fitzgerald DJ, Prior IA, Tepikin AV, Burgoyne RD (2005). Traffic of Kv4 K+ channels mediated by KChIP1 is via a novel post-ER vesicular pathway. J Cell Biol 171, 459–469.

Helenius A, Aebi M (2001). Intracellular functions of N-linked glycans. Science 291, 2364–2369.

Ikeda M, Sugiyama K, Mizutani T, Tanaka T, Tanaka K, Sekihara H, Shimotohno K, Kato N (1998). Human hepatocyte clonal cell lines that support persistent replication of hepatitis C virus. Virus Res 56, 157–167.

Kahn RA, Cherfils J, Elias M, Lovering RC, Munro S, Schurmann A (2006). Nomenclature for the human Arf family of GTP-binding proteins: ARF, ARL, and SAR proteins. J Cell Biol 172, 645–650.

Lavieu G, Zheng H, Rothman JE (2013). Stapled Golgi cisternae remain in place as cargo passes through the stack. Elife 2, e00558.

Lefrancois L, Lyles DS (1982). The interaction of antibody with the major surface glycoprotein of vesicular stomatitis virus. I. Analysis of neutralizing epitopes with monoclonal antibodies. Virology 121, 157–167.

Li K, Chen Z, Kato N, Gale M Jr, Lemon SM (2005). Distinct poly(I-C) and virus-activated signaling pathways leading to interferon-beta production in hepatocytes. J Biol Chem 280, 16739–16747.

Liu S, Hunt L, Storrie B (2013). Rab41 is a novel regulator of Golgi apparatus organization that is needed for ER-to-Golgi trafficking and cell growth. PLoS One 8, e71886.

Mire CE, White JM, Whitt MA (2010). A spatio-temporal analysis of matrix protein and nucleocapsid trafficking during vesicular stomatitis virus uncoating. PLoS Pathog 6, e1000994.

Mironov AA, Beznoussenko GV, Nicoziani P, Martella O, Trucco A, Kweon HS, Di Giandomenico D, Polishchuk RS, Fusella A, Lupetti P, et al. (2001). Small cargo proteins and large aggregates can traverse the Golgi by a common mechanism without leaving the lumen of cisternae. J Cell Biol 155, 1225–1238.

Orci L, Ravazzola M, Volchuk A, Engel T, Gmachl M, Amherdt M, Perrelet A, Sollner TH, Rothman JE (2000). Anterograde flow of cargo across the golgi stack potentially mediated via bidirectional "percolating" COPI vesicles. Proc Natl Acad Sci USA 97, 10400–10405.

Palmer DJ, Helms JB, Beckers CJ, Orci L, Rothman JE (1993). Binding of coatomer to Golgi membranes requires ADP-ribosylation factor. J Biol Chem 268, 12083–12089.

Pereira-Leal JB, Seabra MC (2001). Evolution of the Rab family of small GTP-binding proteins. J Mol Biol 313, 889–901.

Pfeffer SR (2010). How the Golgi works: a cisternal progenitor model. Proc Natl Acad Sci USA 107, 19614–19618.

Presley JF, Cole NB, Schroer TA, Hirschberg K, Zaal KJ, Lippincott-Schwartz J (1997). ER-to-Golgi transport visualized in living cells. Nature 389, 81–85.

Rizzo R, Parashuraman S, Mirabelli P, Puri C, Lucocq J, Luini A (2013). The dynamics of engineered resident proteins in the mammalian Golgi complex relies on cisternal maturation. J Cell Biol 201, 1027–1036.

Seto S, Tsujimura K, Koide Y (2011). Rab GTPases regulating phagosome maturation are differentially recruited to mycobacterial phagosomes. Traffic 12, 407–420.

Sonnichsen B, Lowe M, Levine T, Jamsa E, Dirac-Svejstrup B, Warren G (1998). A role for giantin in docking COPI vesicles to Golgi membranes. J Cell Biol 140, 1013–1021.

Starr T, Sun Y, Wilkins N, Storrie B (2010). Rab33b and Rab6 are functionally overlapping regulators of Golgi homeostasis and trafficking. Traffic 11, 626–636.

Stenmark H, Olkkonen VM (2001). The Rab GTPase family. Genome Biol 2, REVIEWS3007.

Trimble RB, Tarentino AL (1991). Identification of distinct endoglycosidase (endo) activities in Flavobacterium meningosepticum: endo F1, endo F2, and endo F3. Endo F1 and endo H hydrolyze only high mannose and hybrid glycans. J Biol Chem 266, 1646–1651.

Trucco A, Polishchuk RS, Martella O, Di Pentima A, Fusella A, Di Giandomenico D, San Pietro E, Beznoussenko GV, Polishchuk EV, Baldassarre M, et al. (2004). Secretory traffic triggers the formation of tubular continuities across Golgi sub-compartments. Nat Cell Biol 6, 1071–1081.

Velasco A, Hendricks L, Moremen KW, Tulsiani DR, Touster O, Farquhar MG (1993). Cell type-dependent variations in the subcellular distribution of alpha-mannosidase I and II. J Cell Biol 122, 39–51.

Whitt MA, Cox ME, Kansal R, Cox JV (2015). Kinetically distinct sorting pathways through the Golgi exhibit different requirements for Arf1. Traffic 16, 267–283.

Zerial M, McBride H (2001). Rab proteins as membrane organizers. Nat Rev Mol Cell Biol 2, 107–117.